Analysis of Heat Generation and Thermal Lensing in Erbium 3-μm Lasers

Markus Pollnau

Abstract—The influence of energy-transfer upconversion (ETU) between neighboring ions in the upper and lower laser levels of erbium 3-μm continuous-wave lasers on heat generation and thermal lensing is investigated. It is shown that the multiphonon relaxations following each ETU process generate significant heat dissipation in the crystal. This undesired effect is an unavoidable consequence of the efficient energy recycling by ETU in erbium 3-μm crystal lasers, but is further enhanced under nonlasing conditions. Similar mechanisms may affect future erbium 3-μm fiber lasers. In a three-dimensional finite-element calculation, excitation densities, upconversion rates, heat generation, temperature profiles, and thermal lensing are calculated for a $LiYF_4 : Er^{3+}$ 3-μm laser. In the chosen example, the fraction of the absorbed pump power converted to heat is 40% under lasing and 72% under nonlasing conditions. The heat generation in a $LiYF_4 : Er^{3+}$ 3-μm laser is 1.7 and the thermal-lens power up to 2.2 times larger than in a $LiYF_4 : Nd^{3+}$ 1-μm laser under equivalent pump conditions, thus, also putting a higher risk of rod fracture on the erbium system.

Index Terms—Lasers, thermooptic effects.

I. INTRODUCTION

HEAT generation with its undesired consequences of thermal lensing and rod fracture [1]–[6] has become an increasing obstacle to the further power scaling of high-power diode-pumped solid-state lasers. In this respect, high-gain systems with large Stokes efficiencies such as Nd^{3+}- and Yb^{3+}-doped 1-μm lasers provide several advantages over other systems. First, these systems possess a low pump threshold and high power-extraction efficiency and naturally convert a relatively small percentage of the absorbed pump power into heat. Second, these systems can be side pumped, which leads to a relatively uniform heat deposition inside the active medium, or lend themselves to an axial-cooling approach such as the thin-disk concept [7] that avoids strong transverse temperature gradients and consequent thermal lensing. Third, since nonradiative quenching of the upper laser levels of these transitions is weak in many crystalline materials, the choice of host system is governed by power-scaling considerations, and the crystal system with the most suitable thermal and thermo-optical parameters can be chosen. And fourth, the Yb^{3+} ion has a very simple energy-level scheme that avoids parasitic effects [8] such as excited-state absorption (ESA), energy-transfer upconversion (ETU), or cross relaxation (CR) that could induce additional nonradiative decay. This last argument is not necessarily true for Nd^{3+}-doped 1-μm lasers. Under diode end-pumping, ETU processes between neighboring Nd^{3+} ions [9], [10] can lead to significant extra heat dissipation in the crystal [11], [12] when operating this system in a regime of higher excitation density such as a Q-switched laser or an amplifier.

The situation deteriorates noticeably when mid-infrared laser transitions are excited with high-power 800- or 980-nm diode lasers. The Stokes efficiencies in these systems are by far less favorable than in the 1-μm laser systems. (For certain ground-state laser transitions, this fact can be improved by direct upper-state pumping with mid-infrared lasers [13], [14]). The gain cross sections in the mid-infrared Tm^{3+}, Ho^{3+}, Er^{3+}, and other systems are typically an order of magnitude smaller and pump thresholds are usually high. Recent experiments have shown that axial cooling of a mid-infrared thin-disk laser does not deliver improvements similar to those obtained with 1-μm lasers [15]. Furthermore, competition of multiphonon relaxation (MPR) with radiative decay leads to quenched upper-state lifetimes and reduced quantum efficiencies. For transitions above $\sim$ 2.3 μm, minimizing this quenching often requires nonoxide host materials with lower phonon energies but also inferior thermal conductivities and fracture limits compared to oxide materials. Worst of all, the energy-level schemes of these ions are more complex and parasitic effects such as ESA, ETU, and CR often reduce the quantum efficiencies and induce further nonradiative decay and heat dissipation. For future power scaling of mid-infrared lasers, detailed analysis of the population mechanisms for an identification and quantification of the relevant processes will be required in order to understand and possibly circumvent excessive heat dissipation in these systems.

Erbium lasers operating in the mid-infrared spectral region near 3 μm (Fig. 1) are of great interest for specific applications in laser microsurgery [16]–[18] due to the high absorption of 3-μm radiation in water and biological tissue. A number of these applications can be performed with pulsed laser radiation that has been obtained from flashlamp-pumped erbium-doped oxide materials such as $Y_3Al_5O_{12}$ (YAG). These lasers can now be replaced by diode-pumped systems [19]. In specific biomedical applications, high peak powers must be avoided and continuous-wave (CW) radiation with output powers >3 W is required. While ETU from the lower to the upper laser level of erbium [20]–[22] can improve the quantum efficiency at 3 μm by a factor of two [23] compared with short-pulse excitation [24], [25] and CW slope efficiencies beyond the Stokes efficiency of the system have been demonstrated experimentally

M. Pollnau is with the Applied Photonics Laboratory, Institute of Biomedical Imaging, Optics, and Engineering, Swiss Federal Institute of Technology, CH-1015 Lausanne, Switzerland (email: markus.pollnau@epfl.ch).
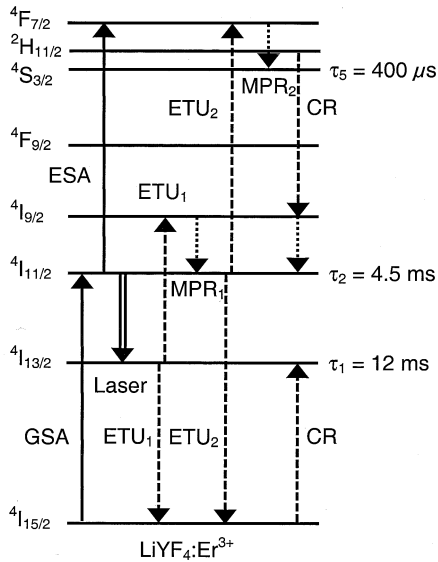
Fig. 1. Energy-level scheme of $LiYF_4 : Er^{3+}$. The dashed lines indicate the relevant energy-transfer transitions and the dotted lines indicate the major multiphonon transitions that contribute to heat dissipation in the crystal.

TABLE I
SPECTROSCOPIC PARAMETERS OF $LiYF_4 : Er^{3+}$. GIVEN ARE THE LIFETIMES τ_i [μs] OF ALL LEVELS, RELEVANT BRANCHING RATIOS β_{ij} [%] OF INTRINSIC DECAY TO LOWER LYING LEVELS, NONRADIATIVE FRACTIONS $\gamma_{i,i-1}$ [%] OF TRANSITIONS $\beta_{i,i-1}$ TO THE NEXT LOWER LYING LEVELS, ENERGIES ΔE [cm^{-1}] CONVERTED TO HEAT BY MULTIPHONON AND ENERGY-TRANSFER PROCESSES, ENERGY-TRANSFER PARAMETERS W_{ij} [cm^{3}s^{-1}], AND PARAMETERS OF THE LASER TRANSITION IN π-POLARIZATION

Linear processes	τ_i	β_{ij}	$\gamma_{i,i-1}$	ΔE
$^4F_{7/2} : \beta_{65}$	2	100	100	2134
$^4S_{3/2} / {}^2H_{11/2} : \beta_{54}, \beta_{53}, \beta_{52}, \beta_{51}, \beta_{50}$	400	30, 2, 1, 18, 49	100	3115
$^4F_{9/2} : \beta_{43}, \beta_{42}, \beta_{40}$	100	90, 1, 9	100	2955
$^4I_{9/2} : \beta_{32}, \beta_{30}$	6.6	99, 1	100	2143
$^4I_{11/2} : \beta_{21}, \beta_{20}$	4500	43, 57	83	3683
$^4I_{13/2} : \beta_{10}$	12000	100	0	6535
ETU processes	W_{ij}	W_{ij}^{-1}		ΔE
$(^4I_{13/2}, {}^4I_{13/2}) \rightarrow ({}^4I_{15/2}, {}^4I_{9/2}): W_{11}$	4.8×10^{-17}	5.3×10^{-18}		400 / -400
$(^4I_{11/2}, {}^4I_{11/2}) \rightarrow ({}^4I_{15/2}, {}^4F_{7/2}): W_{22}$	3.3×10^{-17}	-		0
$(^2H_{11/2}, {}^4I_{15/2}) \rightarrow ({}^4I_{13/2}, {}^4I_{9/2}): W_{50}$	1×10^{-16}	-		-400
Laser transition $^4I_{11/2} \rightarrow {}^4I_{13/2}$	Upper State	Lower State		ΔE
Stark level	2	4		125
Boltzmann factor b_i (300 K)	0.201	0.111		
Degeneracy g_i	2	2		

[26], today's CW output powers at 3 μm are still moderate. The highest output power of 1.8 W was obtained from a diode-pumped erbium-doped $LiYF_4$ (YLF) slab system [27]. These erbium 3-μm CW lasers suffer from strong heat generation and thermal lensing and further power scaling is hampered by the occurrence of rod fracture.

In this paper, a quantitative analysis of the processes that lead to heat generation in a 10-W diode-end-pumped $LiYF_4 : Er^{3+}$ 3-μm laser system is performed. It is shown that part of the heat generation occurs in direct connection with the energy-recycling mechanism, but that significant extra heat is generated under nonlasing conditions. The temperature distributions and thermal-lens powers that result from the thermal input are calculated. Quantitative comparison is made with a $LiYF_4 : Nd^{3+}$ 1-μm laser system under equivalent pump conditions.

II. MODEL PARAMETERS AND EQUATIONS

The computer model used for the simulations of this paper is described in detail in [11]. It solves the equations for the population mechanisms, heat generation, thermal flux, temperature profile, and thermal lensing in the pumped region of the crystal with three-dimensional (3–D) (tangential, sagittal, longitudinal) resolution of 800 finite elements for the tetragonal system $LiYF_4$. Further spatial elements cover the remaining outer parts of the crystal for the calculation of thermal flux, temperature profile, and thermal lensing.

The nonlinear rate equations of the $LiYF_4 : Er^{3+}$ system including all electronic levels from the $^4I_{15/2}$ ground state up to the $^4F_{7/2}$ level (Fig. 1) are taken from [25, eqs. (1)–(6)]. These equations are solved in a Runge–Kutta calculation of fourth order independently for each of the 800 spatial elements in the pumped region. The rate equations consider the relevant processes of the $LiYF_4 : Er^{3+}$ 3-μm laser system such as ground-state absorption (GSA) and ESA, ETU from the two laser levels and CR from the thermally coupled $^4S_{3/2}$ and $^2H_{11/2}$ levels with parameters W_{ij} as well as the inverse process of ETU$_1$

with parameter W_{11}^{-1}, the laser transition, and all fluorescence and MPR transitions from the levels included in the simulation.

In Table I, the relevant spectroscopic parameters of $LiYF_4 : Er^{3+}$ are presented; see [23], [25], [28]–[30], and references therein. The intrinsic lifetimes of the excited levels are given. The branching ratios β_{ij} include radiative and nonradiative parts and are calculated from Judd–Ofelt data for the radiative transition rates in $LiYF_4 : Er^{3+}$ [28] and from the fluorescence lifetimes τ_i with the procedure used in [30]. This procedure assumes that the difference between the total intrinsic decay rate τ_i^{-1} and the sum of the radiative decay rates is due to MPR into the next lower lying level. The nonradiatively emitted fraction of the rate into the next lower lying level is given by $\gamma_{i,i-1}$, i.e., the branching ratio $\beta_{i,i-1}$ splits into a radiative part $(1 - \gamma_{i,i-1}) \beta_{i,i-1}$ and a nonradiative part $\gamma_{i,i-1} \beta_{i,i-1}$. The parameters of the ETU$_1$ process $(^4I_{13/2}, {}^4I_{13/2}) \rightarrow ({}^4I_{15/2}, {}^4I_{9/2})$ from the lower and the ETU$_2$ process $(^4I_{11/2}, {}^4I_{11/2}) \rightarrow ({}^4I_{15/2}, {}^4F_{7/2})$ from the upper laser levels at 15% erbium concentration [29], as well as the CR process $(^2H_{11/2}, {}^4I_{15/2}) \rightarrow ({}^4I_{13/2}, {}^4I_{9/2})$ from the thermally coupled $^4S_{3/2}/^2H_{11/2}$ levels. are given.

In Table II, the relevant data of the $LiYF_4 : Er^{3+}$ crystal, the pump and laser beams, and the resonator are summarized. The pump beam has its waist located at the crystal front surface and diverges on its way through the crystal. The erbium ions are excited at 968 nm by GSA $^4I_{15/2} \rightarrow {}^4I_{11/2}$ and ESA $^4I_{11/2} \rightarrow {}^4F_{7/2}$ [31], [32]. The absorbed fraction of the incident pump power is given for low input power. Absorbed fractions at high pump power are slightly smaller because of ground-state bleaching. It is assumed that after absorption of the pump power

TABLE II
CRYSTAL, PUMP, LASER, AND RESONATOR DATA

Crystal length	6 mm
Crystal radius	2 mm
Er^{3+} conc.	2.07×10^{21} cm^{-3}
	(15 at.%)
Incident pump power	10 W
Pump coupling efficiency	100 %
Pump foci $w_{x,y}$	250 μm
Beam-quality factors $M_{x,y}{}^2$	70
Pump wavelength	968 nm
GSA cross section	2×10^{-21} cm^2
ESA cross section	2×10^{-21} cm^2
Absorbed pump fraction	91.6%
(low pump power)	
Optical resonator length	100 mm
Double-pass losses	1.0%
Mirror reflectance in / out	100% / 98%
Laser wavelength	2.81 μm
Atomic em. cross section	3×10^{-20} cm^2
Eff. em. cross section (300 K)	6×10^{-21} cm^2
TEM$_{00}$ laser-beam radius	250 μm

in each longitudinal element a Gaussian pump shape is maintained, i.e., a possible degradation of the Gaussian pump shape due to ground-state bleaching and a radially nonuniform absorption coefficient is neglected.

The laser transition at 2.81 μm in $LiYF_4 : Er^{3+}$ originates in the second Stark level of the $^4I_{11/2}$ upper laser level and terminates in the fourth Stark level of the $^4I_{13/2}$ lower laser level. For the calculation of the stimulated-emission rate, the following considerations are made. Thermal redistribution within the multiplets takes place instantaneously. Since the temperature profile of the active material is calculated in the simulation, the Boltzmann distributions of upper and lower Stark laser levels are considered with spatial resolution. The temperature-dependent effective emission cross section is the atomic emission cross section weighted by the Boltzmann factor of the upper Stark laser level. The rate equations for the photon number in the resonator and the stimulated-emission rate, given in [11, eqs. (B17) and (B18)], respectively, are modified to represent the laser transition at 2.81 μm in $LiYF_4 : Er^{3+}$.

The approximate energies ΔE converted to heat by each process are presented in Table I. It is assumed that each MPR from level $i \rightarrow i - 1$ (with branching ratio $\gamma_{i,i-1} \beta_{i,i-1}$) is fol-

lowed by intra-multiplet relaxation, i.e., the complete process involves relaxation from lowest to lowest Stark level of the involved multiplets. Each ETU$_1$ process from the lower laser level generates heat, because the emission process involved in the energy transfer has a larger energy gap than the absorption process, leading to the emission of one phonon. Consequently, its inverse process is endothermic, requiring the absorption of one phonon. The ETU$_2$ process from the upper laser level has a direct spectral overlap between the involved emission and absorption processes and can, therefore, be assumed to generate no heat. The cross-relaxation process occurs after thermal excitation of the $^2H_{11/2}$ level and is endothermic, requiring the absorption of one phonon. The laser transition generates heat, because it originates in a low Stark level of $^4I_{11/2}$ and terminates in a high Stark level of $^4I_{13/2}$.

The parameters and values used for the calculation of the temperature profiles and thermal lenses in $LiYF_4$ are summarized in [11]. The dissipated thermal power in each of the 800 spatial elements is calculated from the energy gaps ΔE (Table I) and the rates of the multiphonon, energy-transfer, and stimulated-emission transitions. Radial convective cooling by a water-cooled copper heat sink and convective air cooling at the rod end faces is assumed. The 3-D thermal conduction is considered for the calculation of the temperature distribution in the laser rod, taking into account the anisotropy in the thermal conductivity for the $LiYF_4$ host [33]. The calculation of the thermal lens considers the contributions from the change in refractive index with temperature and the bulging of the rod end faces due to thermal expansion. The temperature dependencies of the thermal conductivity, the change in refractive index with temperature, and the expansion coefficient are also considered [11].

For a direct comparison between the $LiYF_4 : Er^{3+}$ and $LiYF_4 : Nd^{3+}$ systems, it is assumed that the wavelength for pumping a $LiYF_4 : (1.1\%) Nd^{3+}$ crystal near 797 nm is tuned off-peak such that the same absorption length and the same absorbed fraction of 91.6% of the incident pump power (at low pump power) is achieved over the same crystal length of 6 mm as in the $LiYF_4 : (15\%) Er^{3+}$ system. Also, the pump focus and divergence are assumed to be equal (Table II). The relevant spectroscopic parameters of $LiYF_4 : Nd^{3+}$ can be found in [11] and references therein.

III. HEAT GENERATION

The population mechanisms of erbium 3-μm lasers have been discussed in the literature to a large extent. The mechanisms relevant to the investigation of heat generation shall be reviewed here very briefly on the basis of the erbium level scheme of Fig. 1. Direct excitation of the $^4I_{11/2}$ upper laser level at $\sim$970 nm provides the highest Stokes efficiency of $\eta_{Stokes} = 35\%$. At the high erbium concentrations typically present in this laser system, pump ESA is practically negligible [23]. After the laser transition at 2.8 μm, the $^4I_{13/2}$ lower laser level, which possesses a longer lifetime than the upper laser level, must be depleted. The most beneficial way of doing this is by exploiting ETU$_1$ [20], [21]. Half of the ions undergoing this process are excited to $^4I_{9/2}$ and recycled into the upper

laser level by the MPR$_1$ process $^4I_{9/2} \rightarrow {}^4I_{11/2}$, thereby improving the quantum efficiency of the system by a factor of two [23], [34], [42]. The highest slope efficiency is obtained when optimizing the ratio W_{11}/W_{22} [23] of the parameters of ETU$_1$ and the parasitic ETU$_2$ process that depletes the upper laser level. This goal can be reached by optimizing the erbium concentration (to ~15 at % in LiYF$_4$ [22]). The energy that is upconverted by the ETU$_2$ process followed by the MPR$_2$ process $^4F_{7/2} \rightarrow {}^2H_{11/2}/{}^4S_{3/2}$ is recycled to both laser levels by the CR process.

The amount of heat generated by each of the transitions indicated in Fig. 1 is determined by the energy difference ΔE converted to heat by a single transition process (Table I) times the rate at which this process occurs per unit volume. Large energy differences ΔE are converted to heat by the MPR processes (Table I). Also the ETU$_1$ process and the laser transition convert some energy to heat, the ETU$_2$ process is practically inert, whereas the CR process leads to cooling of the crystal, as was discussed in Section II.

At an erbium concentration of 15%, all the energy-transfer processes are typically more efficient than intrinsic decay from the $^4I_{13/2}$, $^4I_{11/2}$, and $^4S_{3/2}/{}^2H_{11/2}$ levels. In addition, the intrinsic decay from these levels is partly radiative ($\gamma_{i,i-1}\,\beta_{i,i-1} \ll 1$; see Table I). As a consequence, heat generation by MPR from these levels occurs at a relatively low rate. Only those levels quenched by fast MPR, i.e., $^4I_{9/2}$, $^4F_{9/2}$, and $^4F_{7/2}$, exhibit a predominant intrinsic decay. $^4F_{9/2}$ is populated mostly by MPR from $^4S_{3/2}$. However, since $^4S_{3/2}/{}^2H_{11/2}$ is depleted mostly by the CR process which bypasses $^4F_{9/2}$, the $^4F_{9/2}$ excitation is small and MPR from this level occurs also at a low rate. In contrast, $^4I_{9/2}$ and $^4F_{7/2}$ are strongly excited by the ETU$_1$ and ETU$_2$ processes, respectively, and decay mostly by fast MPR ($\gamma_{i,i-1}\,\beta_{i,i-1} \approx 1$; see Table I). Each energy-transfer process with its comparatively small exothermic or endothermic heat conversion is followed by a MPR process with large heat generation (ETU$_1$ triggers MPR$_1$, ETU$_2$ triggers MPR$_2$, CR triggers MPR$_1$). Consequently, in each of these chains, the MPR process has practically the same rate as the triggering energy-transfer process and must be the dominant heat-generating process. $^4I_{9/2}$ is populated by both ETU$_1$ as well as the chain ETU$_2$, MPR$_2$, CR, whereas $^4F_{7/2}$ is populated only by ETU$_2$. In addition, the erbium concentration was chosen such as to achieve an optimized ratio W_{11}/W_{22}. It follows that MPR$_1$ has a higher rate than MPR$_2$, while both processes have similar energy differences ΔE. This identifies MPR$_1$ as the largest and MPR$_2$ as the second largest heat-generating process in the erbium system.

Fig. 2 indicates the thermal power generated by each of the major transitions that contribute to heat dissipation in LiYF$_4$: Er^{3+} in the region of the highest pump absorption (front surface, center of the pump beam) versus incident pump power, calculated from the rate equations under 3-μm lasing and nonlasing conditions. In an erbium 3-μm laser system (open symbols) optimized for high slope efficiency and diode-end-pumped with 10 W of incident power, 108 mW or 44% of the pump power of 246 mW absorbed in this region of the crystal is converted to heat. Since at higher pump powers the ETU processes dominate over intrinsic decay for the depletion of the laser levels,
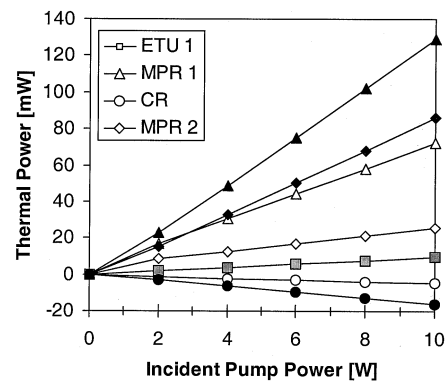

Fig. 2. Calculated thermal power generated by the major transitions that contribute to heat dissipation in LiYF$_4$:Er^{3+} at the front surface (first 0.5 mm) and in the center of the pump beam (square of $120 \times 120 \ \mu$m^2) versus incident pump power under 3-μm lasing (open symbols) and nonlasing (solid symbols) conditions. The rate of ETU$_1$ is very similar under lasing and nonlasing conditions and the thermal power generated by this process is displayed in gray.

these and all other relevant processes and, thus, also the heat generation tend to become linear with pump power [35]. The largest amount of heat is indeed generated by MPR$_1$ (triangles), followed by MPR$_2$ (diamonds). ETU$_1$ and CR have a smaller influence because each such process generates or removes a significantly smaller amount of heat. Under nonlasing conditions (solid symbols), the $^4I_{11/2}$ upper laser level is not clamped to laser threshold and builds up a significantly larger population density compared to 3-μm lasing conditions, thereby increasing the rates of the ETU$_2$ and subsequent MPR$_2$, CR, and MPR$_1$ processes, i.e., the rates of MPR$_2$ and MPR$_1$ increase by similar amounts, and so does the heat generated by these two processes (because of similar ΔE). Cooling by the CR process increases accordingly, whereas the ETU$_1$ process is not much affected (gray symbols for lasing and nonlasing conditions). In total, 86% of the pump power absorbed in the region of the highest pump absorption is converted to heat, significantly more than under lasing conditions.

When comparing the pump powers converted to heat in the whole crystals for the same incident and absorbed pump powers in LiYF$_4$: Er^{3+} and LiYF$_4$: Nd^{3+} (Fig. 3), we find that the erbium 3-μm laser generates ~1.7 times more heat than the neodymium 1-μm laser (3.7 W or 40% versus 2.2 W or 24% for 9.2 W of absorbed pump power). Thus, the risk of rod fracture is much higher in the erbium-laser system. Under nonlasing conditions, the situation worsens for both systems. However, the ratio decreases to ~1.35 (6.6 W or 72% versus 4.9 W or 53%), because the power extraction in neodymium by the 1-μm laser transition is efficient and the influence of ETU and subsequent MPR is practically negligible under lasing conditions, i.e., the difference between lasing and nonlasing conditions is more pronounced than in the erbium system.

The erbium-doped 3-μm fluoride-fiber laser [34], [42] represents a promising alternative for the construction of a compact high-power diode-pumped efficient mid-infrared laser. Due to its large surface-to-volume ratio and consequent better cooling, the optical fiber provides potentially higher pump and output powers than the bulk system without the drawbacks of thermal and thermo-optical effects. Nevertheless, significant heat is also
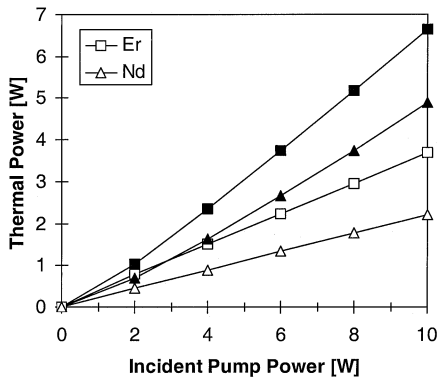
Fig. 3. Calculated thermal power dissipated in the whole crystal versus incident pump power under 3-μm lasing (open symbols) and nonlasing (solid symbols) conditions for LiYF$_4$: Er^{3+} (squares) and LiYF$_4$: Nd^{3+} (triangles). The absorbed fraction of pump power is approximately 92% for all curves.

generated in this system. The lifetime-quenching regime [36] that is achieved by co-doping the fiber with Pr^{3+} ions has so far produced the highest reported output power of 1.7 W from a fiber laser at 3 μm [37]. The MPR that occurs within Pr^{3+} after energy transfer from the lower laser level of Er^{3+} generates an amount of heat, which is $1 - \eta_{\mathrm{Stokes}} = 65\%$ of the absorbed 975-nm pump power in the ideal case and may further increase if parasitic processes come in.

The energy-recycling regime that was recently proposed for the fiber system [38] generates heat in the same way as the crystal system investigated in this paper, i.e., only ~40% of the absorbed pump power, because it relies on the same ETU processes [39] as the crystal system. However, since a high erbium concentration is required for efficient ETU, resulting in higher pump absorption, one of the great advantages of the fiber host—the long interaction length and consequent better distribution of the generated heat—may be lost. Although the effect of a larger absorbed pump-power density can be compensated by a smaller core-area/pump-cladding-area ratio, leading to a reduced effective absorption coefficient, such a compensation finds its limitation in either the increase in core temperature that results from the longer distance to the cooled surface (when increasing the cladding area) or possible fiber or mirror damage owing to the increase in oscillating signal intensity at 3 μm [38] (when reducing the core area). As average pump and output powers increase, thermal and thermo-optical effects start to play a role also in double-clad fiber lasers [40]. Since the thermo-optical properties of fluoride glasses [41] are inferior to those of silica glasses, such effects will probably have to be taken into account when future high-output-power erbium-doped 3-μm fluoride-fiber lasers are constructed.

IV. TEMPERATURE PROFILES AND THERMAL LENSING

The large amount of pump-induced heating requires cooling of the laser crystal. Radial convective cooling by a copper heat sink (and surface convective cooling by air which has only a small influence) are assumed in the calculation. The temperature profiles arising from the Gaussian pump shape, the nonlinear heat dissipation, the temperature-dependent thermal conductivity, and the radial cooling are calculated under lasing and nonlasing conditions for different pump powers. The sagittal
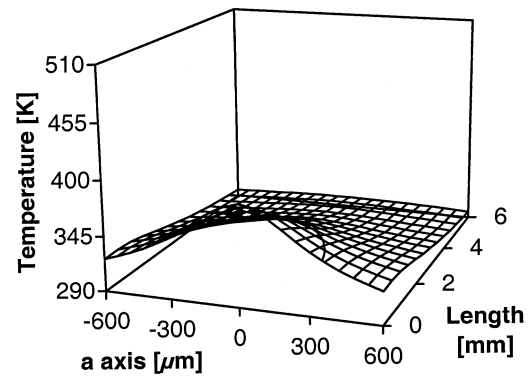
(a)
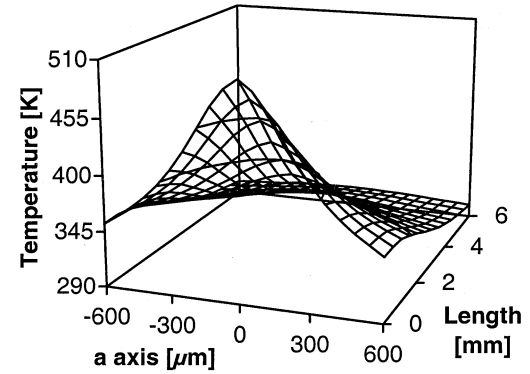
(b)

Fig. 4. Calculated temperature profiles in LiYF$_4$: Er^{3+} versus crystal a axis (pump- and laser-beam waists 250 μm) and length under (a) 3-μm lasing and (b) nonlasing conditions at an incident pump power of 10 W. The radial boundary given by the rod radius is at ± 2 mm. Owing to the assumption of convective radial cooling by a water-cooled copper block, the temperature at the rod boundary is elevated from the radial coolant temperature of 288 K by a few Kelvins.

and longitudinal temperature profiles in LiYF$_4$: Er^{3+} at the highest incident pump power of 10 W are shown in Fig. 4. The largest temperature increase is found at the crystal front surface in the center of the pump beam where the strongest absorption occurs. The temperature increase from the coolant temperature of 288 K by ~100 K under lasing conditions [Fig. 4(a)] is already significant, but is further increased under nonlasing conditions [Fig. 4(b)] to reach ~210 K at the point of highest pump absorption. Such strong temperature gradients can easily lead to rod fracture in LiYF$_4$.

The corresponding temperature increase in LiYF$_4$: Nd^{3+} for 10 W of incident pump power is only ~50 K and ~140 K under lasing and nonlasing conditions, respectively. The significantly larger temperature increase in LiYF$_4$: Er^{3+} is the result of the larger heat generation in this system and the unfavorable temperature dependence of the thermal conductivity.

The transverse temperature gradient that results from radial cooling induces strong thermal lensing in the crystal. Three different effects are generally important in this context. First, the refractive index of the host material changes with temperature, which leads to differences in longitudinal optical path lengths through the rod across the transverse temperature profile, thus introducing a lens whose power has the same sign as the change of refractive index with temperature. Second, the crystal expands with temperature and the resulting bulging of the rod end
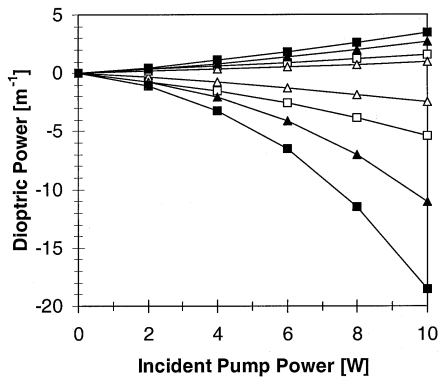
Fig. 5. Calculated dioptric power of the thermal lens along the crystal a axis for $LiYF_4 : Er^{3+}$ (squares) and $LiYF_4 : Nd^{3+}$ (triangles) under lasing conditions (open symbols) at 3 and 1 μm, respectively, and nonlasing conditions (solid symbols) in σ (upper four curves) and π (lower four curves) polarization versus incident pump power.

faces defines a lens which has the same sign as the expansion of the crystal along the resonator axis. Third, the nonuniform expansion leads to stress in the crystal, which also changes the refractive index, leading to stress-induced birefringence. This last effect is not considered in the calculation. It is believed to be of minor importance in $LiYF_4$ [4], because this material shows a strong natural birefringence. Since the temperature increase in the rod is significant under high-power end-pumping, a knowledge of the temperature dependence not only of the thermal conductivity but also of the thermo-optical parameters (change in refractive index with temperature, expansion coefficient) is important and has been taken into account in the simulation in the same way as in [11].

In $LiYF_4$, there are four principal values of thermal lens, depending on the choice of lens axis, c or a, and on the choice of polarization, π or σ (parallel and perpendicular to the crystal c axis, respectively). The calculated results for the a axis in $LiYF_4 : Er^{3+}$ (squares) and $LiYF_4 : Nd^{3+}$ (triangles) are shown in Fig. 5. The thermal-lens powers under lasing (open symbols) and especially under nonlasing (solid symbols) conditions increase nonlinearly with pump power. The contribution to the thermal-lens power from the change in refractive index with temperature is negative. For π polarization, its absolute value is larger than that from the bulging of the rod end faces, resulting in negative thermal-lens powers. For σ polarization, the contribution from the change in refractive index with temperature is smaller in absolute value and the bulging effect predominates, resulting in a positive sign of the thermal lens.

The thermal-lens powers generated in the erbium system are 1.3 (σ polarization, nonlasing) to 2.2 (π polarization, lasing) times larger than in the neodymium system. The additional heat generated in the crystal under nonlasing conditions, in combination with the unfavorable temperature dependencies of thermal conductivity and thermo-optical parameters, leads to much stronger thermal-lens powers compared to lasing conditions. At the highest incident pump power of 10 W, the thermal-lens power in $LiYF_4 : Er^{3+}$ under nonlasing conditions compared to lasing conditions is $\sim$3.4 times stronger in π polarization and $\sim$2.2 times stronger in σ polarization. The difference in this factor for the two polarizations is a

consequence of the different temperature dependence of the change in refractive index and thermal expansion coefficient. For $LiYF_4 : Nd^{3+}$, the difference between nonlasing and lasing conditions is even larger ($\sim$4.4 times in π polarization and $\sim$2.9 times in σ polarization) because of the larger difference in heat generation. The values presented in Fig. 5 are averaged over the spot size of the oscillating laser beam of 250-μm radius.

Strong spherical aberrations of the thermal lens occur that increase with average thermal-lens power. These aberrations lead to a distortion of the Gaussian shape of the fundamental laser mode, with a consequent degradation in laser-beam quality. At a critical power level, a small increase in pump power can lead to a partly unstable resonator with higher resonator losses. With all the nonlinearities involved in the system, a dramatic change in the behavior from lasing to nonlasing condition results, followed by a catastrophic increase in temperature and rod fracture.

With the expectation of such dramatic effects in mind, further parameter variations were performed to investigate their impact on laser operation, heat generation, and thermal lensing. For example, a simultaneous decrease of the pump- and laser-beam waists from 250 to 100 μm slightly increases the output power from 2.4 to 3.0 W due to a larger ETU_1 rate and improved energy recycling from lower to upper laser level, which also leads to a slight reduction in heat generation from 3.7 to 3.6 W. However, owing to the stronger confinement of the heat deposition the thermal-lens power increases dramatically, e.g., along the crystal a axis in π polarization from -5.4 to -34.7 m^{-1}. An increase of the resonator losses from 0% to 5%, e.g., by slight misalignment of a resonator mirror or resonator instabilities owing to increased thermal lensing, implies a decrease in output power of this low-gain laser system from 3.9 to 0.6 W. The simultaneous increase in the population of the upper laser level significantly enhances the rates of ETU_2, MPR_2, CR, and MPR_1. As a consequence, the heat generated in the whole crystal increases from 3.4 to 4.8 W. This additional heat induces a large increase in the thermal-lens power, e.g., along the crystal a axis in π polarization from -4.9 to -9.0 m^{-1}. Such increases in heat generation and thermal-lens power as calculated in the above examples can easily lead to resonator instabilities and rod fracture.

V. CONCLUSION

It has been shown in this paper that the ETU processes that are typical of the population mechanisms of erbium 3-μm lasers do not contribute much to heat generation themselves. However, they bear responsibility for triggering nonradiative decay by MPR processes that dissipate large amounts of heat in the crystal. The situation worsens significantly under nonlasing compared to lasing conditions because of the increased population density in the upper laser level, leading to additional ETU. The resulting increase in temperature and thermal-lens powers provides a good understanding why this laser system is quite frequently reported to suffer from rod fracture, especially when comparing its performance with other rare-earth-doped solid-state lasers under equivalent pump conditions.

Generally, there are several ways to limit the influence of ETU and heat generation by subsequent MPR. One way is to use

a smaller dopant concentration. This decreases energy migration within the initial level of the upconversion process and hence the possibility of two excitations to meet at nearest-neighbor distance. Thus, the ETU parameter decreases. In addition, the excitation density under the same pump conditions is smaller. Other possibilities to decrease the excitation density and influence of ETU are to tune the pump to a wavelength with smaller absorption cross section or to choose a larger pump-waist size. These measures are less powerful than the first, because they do not simultaneously decrease the upconversion parameter. All these measures may be successful in the case of a neodymium 1-μm laser, however, in an erbium 3-μm laser they imply a decrease in energy recycling from lower to upper laser level by ETU and a corresponding decrease in slope efficiency and overall performance of the system. It is an unfortunate circumstance that significant extra heat generation unavoidably comes along with efficient energy recycling in erbium 3-μm lasers.

Although the erbium 3-μm laser represents only a specific example of the large class of current and future diode-pumped mid-infrared lasers, it displays some of the difficulties that can arise when a mid-infrared laser transition either occurs between two excited states or terminates in the ground state but a suitable mid-infrared pump source is not at hand, both resulting in a rather low Stokes efficiency of the system.

REFERENCES

[1] M. E. Innocenzi, H. T. Yura, C. L. Fincher, and R. A. Fields, "Thermal modeling of continuous-wave end-pumped solid-state lasers," *Appl. Phys. Lett.*, vol. 56, no. 19, pp. 1831–1833, 1990.

[2] S. C. Tidwell, J. F. Seamans, M. S. Bowers, and A. K. Cousins, "Scaling CW diode-end-pumped Nd:YAG lasers to high average powers," *IEEE J. Quantum Electron.*, vol. 28, pp. 997–1009, Apr. 1992.

[3] A. K. Cousins, "Temperature and thermal stress scaling in finite-length end-pumped laser rods," *IEEE J. Quantum Electron.*, vol. 28, pp. 1057–1069, Apr. 1992.

[4] C. Pfistner, R. Weber, H. P. Weber, S. Merazzi, and R. Gruber, "Thermal beam distortions in end-pumped Nd:YAG, Nd:GSGG, and Nd:YLF rods," *IEEE J. Quantum Electron.*, vol. 30, pp. 1605–1615, July 1994.

[5] U. Brauch, "Temperature dependence of efficiency and thermal lensing of diode-laser-pumped Nd:YAG lasers," *Appl. Phys. B*, vol. 58, no. 5, pp. 397–402, 1994.

[6] M. Lukač and M. Marincek, "Energy storage and heat deposition in flashlamp-pumped sensitized erbium glass lasers," *IEEE J. Quantum Electron.*, vol. 26, pp. 1779–1787, Oct. 1990.

[7] A. Giesen, H. Hügel, A. Voss, K. Wittig, U. Brauch, and H. Opower, "Scalable concept for diode-pumped high-power solid-state lasers," *Appl. Phys. B*, vol. 58, no. 5, pp. 365–372, 1994.

[8] T. Y. Fan, "Heat generation in Nd:YAG and Yb:YAG," *IEEE J. Quantum Electron.*, vol. 29, pp. 1457–1459, June 1993.

[9] Y. Guyot, H. Manaa, J. Y. Rivoire, R. Moncorgé, N. Garnier, E. Descroix, M. Bon, and P. Laporte, "Excited-state absorption and upconversion studies of Nd^{3+}-doped single crystals Y$_3$Al$_5$O$_{12}$, YLiF$_4$, and LaMgAl$_{11}$O$_{19}$," *Phys. Rev. B*, vol. 51, no. 2, pp. 784–799, 1995.

[10] M. Pollnau, P. J. Hardman, W. A. Clarkson, and D. C. Hanna, "Upconversion, lifetime quenching, and ground-state bleaching in Nd^{3+} : LiYF$_4$," *Opt. Commun.*, vol. 147, no. 1–3, pp. 203–211, 1998.

[11] M. Pollnau, P. J. Hardman, M. A. Kern, W. A. Clarkson, and D. C. Hanna, "Upconversion-induced heat generation and thermal lensing in Nd:YLF and Nd:YAG," *Phys. Rev. B*, vol. 58, no. 24, pp. 16 076–16 092, 1998.

[12] P. J. Hardman, W. A. Clarkson, G. J. Friel, M. Pollnau, and D. C. Hanna, "Energy-transfer upconversion and thermal lensing in high-power end-pumped Nd:YLF laser crystals," *IEEE J. Quantum Electron.*, vol. 35, pp. 647–655, Apr. 1999.

[13] C. D. Nabors, J. Ochoa, T. Y. Fan, A. Sanchez, H. K. Choi, and G. W. Turner, "Ho:YAG laser pumped by 1.9-μm diode lasers," *IEEE J. Quantum Electron.*, vol. 31, pp. 1603–1605, Sept. 1995.

[14] C. Bollig, R. A. Hayward, W. A. Clarkson, and D. C. Hanna, "2-W Ho:YAG laser intracavity pumped by a diode-pumped Tm:YAG laser," *Opt. Lett.*, vol. 23, no. 22, pp. 1757–1759, 1998.

[15] A. Giesen, "Private communication," unpublished.

[16] M. Krause, D. Steeb, H. J. Foth, J. Weindler, and K. W. Ruprecht, "Ablation of vitreous tissue with erbium:YAG laser," *Invest. Ophtalmol. Vis. Sci.*, vol. 40, no. 6, pp. 1025–1032, 1999.

[17] M. P. Goldman, N. Marchell, and R. E. Fitzpatrick, "Laser skin resurfacing of the face with a combined CO$_2$/Er:YAG laser," *Dermatol. Surg.*, vol. 26, no. 2, pp. 102–104, 2000.

[18] T. Wesendahl, P. Janknecht, B. Ott, and M. Frenz, "Erbium:YAG laser ablation of retinal tissue under perfluorodecaline: determination of laser-tissue interaction in pig eyes," *Invest. Ophtalmol. Vis. Sci.*, vol. 41, no. 2, pp. 505–512, 2000.

[19] C. Ziolek, H. Ernst, G. F. Will, H. Lubatschowski, H. Welling, and W. Ertmer, "High-repetition-rate, high-average-power, diode-pumped 2.94-μm Er:YAG laser," *Opt. Lett.*, vol. 26, no. 9, pp. 599–601, 2001.

[20] K. S. Bagdasarov, V. I. Zhekov, V. A. Lobachev, T. M. Murina, and A. M. Prokhorov, "Steady-state emission from a Y$_3$Al$_5$O$_{12}$: Er$_{3+}$ laser ($\lambda = 2.94\,\mu$, $T = 300°K$)," *Sov. J. Quantum Electron.*, vol. 13, no. 2, pp. 262–263, 1983.

[21] D. S. Knowles and H. P. Jenssen, "Upconversion versus Pr-deactivation for efficient 3 μm laser operation in Er," *IEEE J. Quantum Electron.*, vol. 28, pp. 1197–1208, Apr. 1992.

[22] T. Jensen, A. Diening, G. Huber, and B. H. T. Chai, "Investigation of diode-pumped 2.8-μm Er : LiYF$_4$ lasers with various doping levels," *Opt. Lett.*, vol. 21, no. 8, pp. 585–587, 1996.

[23] M. Pollnau, R. Spring, C.Ch. Ghisler, S. Wittwer, W. Lüthy, and H. P. Weber, "Efficiency of erbium 3-μm crystal and fiber lasers," *IEEE J. Quantum Electron.*, vol. 32, pp. 657–663, Apr. 1996.

[24] A. M. Prokhorov, V. I. Zhekov, T. M. Murina, and N. N. Plantov, "Pulsed YAG : Er^{3+} laser efficiency (analysis of model equations)," *Laser Phys.*, vol. 3, no. 1, pp. 79–83, 1993.

[25] M. Pollnau, R. Spring, S. Wittwer, W. Lüthy, and H. P. Weber, "Investigations on the slope efficiency of a pulsed 2.8-μm Er^{3+} : LiYF$_4$ laser," *J. Opt. Soc. Amer. B*, vol. 14, no. 4, pp. 974–978, 1997.

[26] C. Wyss, W. Lüthy, H. P. Weber, P. Rogin, and J. Hulliger, "Emission properties of an optimized 2.8 μm Er^{3+} : YLF laser," *Opt. Commun.*, vol. 139, no. 4–6, pp. 215–218, 1997.

[27] A. Y. Dergachev, J. H. Flint, and P. F. Moulton, "1.8-W CW Er:YLF diode-pumped laser," in *OSA Conf. Lasers and Electro-Optics Tech. Dig.*. Washington, DC, 2000, p. 564.

[28] C. Li, Y. Guyot, C. Linarès, R. Moncorgé, and M. F. Joubert, "Radiative transition probabilities of trivalent rare-earth ions in LiYF$_4$," in *OSA Proceedings on Advanced Solid-State Lasers*, A. A. Pinto and T. Y. Fan, Eds. Washington, DC: Optical Society of America, 1993, vol. 15, pp. 91–95.

[29] T. Jensen, "Upconversion-Prozesse und Wirkungsquerschnitte in Er^{3+}-dotierten 3 μm Fluorid- und Granat-Lasern, gepumpt mit cw und quasi-cw Dioden-Arrays," Ph.D. dissertation, Institute of Laser-Physics, University of Hamburg, Germany, 1996.

[30] M. Pollnau, Th. Graf, J. E. Balmer, W. Lüthy, and H. P. Weber, "Explanation of the cw operation of the Er^{3+} 3-μm crystal laser," *Phys. Rev. A*, vol. 49, no. 5, pp. 3990–3996, 1994.

[31] T. Danger, J. Koetke, R. Brede, E. Heumann, G. Huber, and B. H. T. Chai, "Spectroscopy and green upconversion laser emission of Er^{3+}-doped crystals at room temperature," *J. Appl. Phys.*, vol. 76, no. 3, pp. 1413–1422, 1994.

[32] M. Pollnau, W. Lüthy, H. P. Weber, K. Krämer, H. U. Güdel, and R. A. McFarlane, "Excited-state absorption in Er : BaY$_2$F$_8$ and Cs$_3$Er$_2$Br$_9$ and comparison with Er : LiYF$_4$," *Appl. Phys. B*, vol. 62, no. 4, pp. 339–344, 1996.

[33] B. W. Woods, S. A. Payne, J. E. Marion, R. S. Hughes, and L. E. Davis, "Thermomechanical and thermo-optical properties of the LiCaAlF$_6$: Cr^{3+} laser material," *J. Opt. Soc. Amer. B*, vol. 8, no. 5, pp. 970–977, 1991.

[34] M. Pollnau and S. D. Jackson, "Erbium 3-μm fiber lasers," *IEEE J. Select. Topics Quantum Electron.*, vol. 7, pp. 30–40, Jan./Feb. 2001.

[35] M. Pollnau, D. R. Gamelin, S. R. Lüthi, H. U. Güdel, and M. P. Hehlen, "Power dependence of upconversion luminescence in lanthanide and transition-metal-ion systems," *Phys. Rev. B*, vol. 61, no. 5, pp. 3337–3346, 2000.

[36] M. Pollnau, "The route toward a diode-pumped 1-W erbium 3-μm fiber laser," *IEEE J. Quantum Electron.*, vol. 33, pp. 1982–1990, Nov. 1997.

[37] S. D. Jackson, T. A. King, and M. Pollnau, "Diode-pumped 1.7-W erbium 3-μm fiber laser," *Opt. Lett.*, vol. 24, no. 16, pp. 1133–1135, 1999.

[38] M. Pollnau and S. D. Jackson, "Energy recycling versus lifetime quenching in erbium-doped 3-μm fiber lasers," *IEEE J. Quantum Electron.*, vol. 38, pp. 162–169, Feb. 2002.

[39] P. S. Golding, S. D. Jackson, T. A. King, and M. Pollnau, "Energy-transfer processes in Er^{3+}-doped and Er^{3+},Pr^{3+}-codoped ZBLAN glasses," *Phys. Rev. B*, vol. 62, no. 2, pp. 856–864, 2000.

[40] D. C. Brown and H. J. Hoffman, "Thermal, stress, and thermo-optic effects in high average power double-clad silica fiber lasers," *IEEE J. Quantum Electron.*, vol. 37, pp. 207–217, Feb. 2001.

[41] S. M. Lima, T. Catunda, R. Lebullenger, A. C. Hernandes, M. L. Baesso, A. C. Bento, and L. C. M. Miranda, "Temperature dependence of thermo-optical properties of fluoride glasses determined by thermal lens spectrometry," *Phys. Rev. B*, vol. 60, no. 22, pp. 15 173–15 178, 1999.

[42] M. Pollnau and S. D. Jackson, "Correction to "Erbium 3-μm fiber lasers"," *IEEE J. Select. Topics Quantum Electron.*, vol. 8, p. 956, July/Aug. 2002.

Markus Pollnau received the Diploma in physics from the University of Hamburg, Hamburg, Germany, in 1992 and the Ph.D. in physics from the University of Bern, Bern, Switzerland, in 1996.

From 1996 to 1998, he was with the University of Southampton, Southampton, U.K., as a Research Fellow of the European Union, and from 1998 to 1999 with the University of Bern. From 1998 to 2000, he was also a Visiting Researcher at the University of Manchester, Manchester, U.K. In 1999, he joined the Applied Photonics Laboratory, Institute of Biomedical Imaging, Optics, and Engineering (formerly the Institute of Applied Optics), Swiss Federal Institute of Technology, Lausanne, as a Profil Fellow of the Swiss National Science Foundation. His current research interests are in the fields of broadband light sources based on transition-metal-ion and rare-earth-ion doped waveguide structures for applications in optical coherence tomography and mid-infrared fiber lasers for applications in microsurgery. He has coauthored over 100 technical contributions in international journals and conferences.

Dr. Pollnau is a Member of the European, German, and Swiss Physical Societies and the Optical Society of America.